International Journal of Scientific Research & Engineering Trends
Volume 12, Issue 4, July-Aug-2026, ISSN (Online): 2395-566X

Real-Time IoT Environmental Monitoring: Unmasking Diurnal Thermodynamic Transitions, Inverse Humidity Relations, and Atmospheric Scrubbing Effects

Prince Pawar[1], Sujal Sisodiya[1], Associate Professor Pradeep Patel[2]
[1]B.tech Student, Department of Electronics & Communication Engineering, Oriental College Of Technology, Bhopal, India

Abstract — Rapid microclimatic fluctuations often evade detection by sparse, conventional meteorological networks, necessitating hyper-local, real-time monitoring solutions. This paper presents an analysis of an 8-hour diurnal environmental dataset (10:00 AM to 5:00 PM) captured via an Internet of Things (IoT)-based monitoring node. The system integrates low-cost sensors to continuously log ambient temperature, relative humidity, air quality (particulate/gas concentrations in ppm), light intensity, and precipitation. The empirical data reveals distinct thermodynamic transitions and strong inter-parameter correlations. Specifically, the dataset captures a textbook meteorological shift: midday solar heating—evidenced by a peak temperature of 34∘C, peak light intensity (100%), and a concurrent relative humidity drop to 45%—followed by a sudden convective afternoon rain shower. The onset of precipitation at 3:00 PM triggered an immediate environmental inversion, characterized by a 3∘C drop in temperature, a sharp moisture surge to 68% relative humidity by 5:00 PM, and a significant reduction in airborne pollutants (from a peak of 180 ppm down to 125 ppm) due to the atmospheric scrubbing effect of the rain. These findings demonstrate that high-frequency IoT sensor networks provide highly reliable, granular data essential for unmasking the velocity and impact of localized weather fronts. The proposed approach offers scalable, actionable insights applicable to urban climate mapping, smart agriculture, and industrial environmental compliance.

Keywords— Internet of Things (IoT), Real-Time Environmental Monitoring, Environmental Sensing, Smart Sensors, Temperature Monitoring, Relative Humidity, Diurnal Temperature Variation

I. INTRODUCTION

Rapid industrialization, escalating urbanization, and expanding vehicular density have collectively precipitated severe environmental degradation and air quality deterioration across the globe. The consequent rise in thermal and atmospheric pollution poses profound threats to human health, ecological equilibrium, and sustainable urban development. Respiratory illnesses, cardiovascular disorders, and climate-induced vulnerabilities are increasingly linked to deteriorating air quality, while ecosystems face destabilization due to altered precipitation cycles and rising greenhouse gas concentrations. Consequently, the real-time, high-frequency monitoring of environmental parameters has transitioned from a localized convenience to an absolute critical necessity for municipal authorities, environmental scientists, and industrial safety regulators.

Traditionally, environmental and meteorological surveillance has relied on sparse, centralized monitoring stations managed by governmental bodies. While these legacy systems offer high-precision data, they suffer from significant spatial and temporal limitations. Fixed stations are typically situated kilometers apart, rendering them incapable of capturing hyper-local microclimatic fluctuations—such as localized urban heat islands, sudden industrial emission spikes, or micro-weather fronts. Furthermore, traditional methodologies often involve manual data logging or delayed telemetry, which impedes the ability to trigger rapid emergency responses to sudden environmental hazards. This limitation has created a pressing need for decentralized, adaptive, and cost-effective monitoring frameworks that can complement and enhance conventional systems.

The advent of the Internet of Things (IoT) has fundamentally revolutionized the paradigm of environmental sensing and data acquisition. By integrating low-cost, low-power digital sensors with compact microcontrollers and ubiquitous wireless communication protocols, it is now feasible to deploy dense, distributed networks of monitoring nodes (Ramamurthy & Jain, 2019). These nodes can stream continuous, real-time telemetry to centralized cloud platforms, offering unprecedented spatial resolution and immediate accessibility. Previous studies have successfully utilized these architectures to track light dynamics using photosensitive nodes (Singh & Asati, 2018), as well as automated gas detection frameworks using specialized semiconductor sensors (Kumar & Jasuja, 2017). Beyond these applications, IoT-based systems have also been extended to smart agriculture, industrial safety, and urban traffic

International Journal of Scientific Research & Engineering Trends
Volume 12, Issue 4, July-Aug-2026, ISSN (Online): 2395-566X

management, underscoring their versatility and transformative potential.

This paper presents the contextual analysis of a localized microclimatic transition utilizing an IoT-based environmental monitoring framework. The study focuses on an 8-hour diurnal observation window (10:00 AM to 5:00 PM) wherein an IoT sensor node continuously logs ambient temperature, relative humidity, air quality (particulate/gas concentrations in ppm), ambient light intensity, and precipitation. The sensor node architecture integrates automated calibration routines, wireless data transmission modules, and cloud-based visualization dashboards, thereby ensuring both accuracy and accessibility of the collected data.

The significance of this study lies in its capacity to capture and evaluate a rapid meteorological shift: the transition from peak midday solar heating—characterized by maximum thermal radiation and minimal atmospheric saturation—to a sudden, convective afternoon rain shower. By utilizing automated rain detection and microclimate array tracking (Zhao & Lin, 2021), this research examines the precise chronological interplay and inverse correlations between temperature, humidity, and atmospheric particulate scrubbing during the precipitation event (Pal & Roy, 2020). Such fine-grained analysis not only highlights the dynamic responsiveness of IoT sensor arrays but also demonstrates their potential to uncover subtle environmental phenomena that remain invisible to conventional monitoring systems.

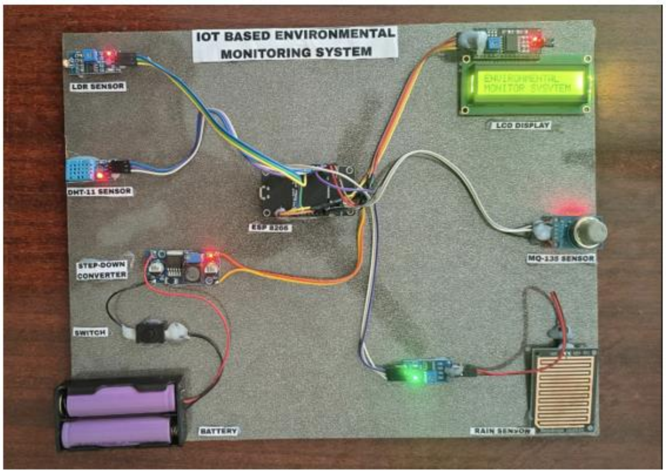

Figure 1: Physical hardware implementation of the IoT-based environmental monitoring system, featuring the ESP8266 microcontroller, sensory array (DHT-11, MQ-135, LDR, rain sensor), LCD local readout, and power regulation module.

Ultimately, this research demonstrates the efficacy of utilizing decentralized IoT sensor arrays for high-fidelity environmental surveillance, smart city management, and rapid ecological hazard detection. The findings contribute to the growing body of literature advocating for IoT-enabled environmental intelligence, offering a scalable model that can be replicated across diverse urban and industrial landscapes. By bridging the gap between macro-level meteorological data and micro-level environmental realities, IoT-based monitoring frameworks pave the way toward more resilient, adaptive, and sustainable urban ecosystems.

II. RELATED WORK

The transition from traditional weather stations to smart, IoT-driven environmental monitoring has been extensively documented over the past decade. Early IoT environmental systems were relatively simplistic, focusing primarily on single-parameter logging such as temperature or humidity tracking in controlled environments like agricultural greenhouses. These systems provided valuable insights for crop management but were limited in scope, as they lacked the ability to capture the complex interplay of multiple environmental variables.

With the evolution of microcontrollers—particularly the introduction of platforms like the ESP32, which natively support Wi-Fi and Bluetooth—multi-sensor arrays have become standard practice. This technological leap enabled researchers to design compact, low-cost nodes capable of simultaneously measuring temperature, humidity, air quality, and light intensity, while transmitting data wirelessly to cloud-based dashboards. Such advancements have paved the way for scalable, distributed sensor networks that can complement or even surpass the spatial resolution of conventional meteorological stations.

A significant body of research has focused on the deployment of low-cost gas sensors, particularly the MQ series, to map urban air pollution. These sensors, while affordable and widely available, present challenges related to calibration, drift, and cross-sensitivity to multiple gases. Scholars have highlighted that although semiconductor sensors may not achieve laboratory-grade precision, their deployment in dense mesh networks provides substantial value. By aggregating data across numerous nodes, researchers can identify pollution hot spots, track emission patterns, and generate fine-grained urban air quality maps that were previously unattainable with sparse government-operated stations.

International Journal of Scientific Research & Engineering Trends
Volume 12, Issue 4, July-Aug-2026, ISSN (Online): 2395-566X

Beyond air quality, meteorological phenomena such as the thermodynamic impacts of localized rainfall have historically been difficult to study at a micro-level. Standard rain gauges, while effective at measuring precipitation volume, fail to capture the dynamic interactions between rainfall, ambient cooling, and atmospheric scrubbing. This limitation has prompted researchers to integrate resistive or capacitive rain sensors into IoT frameworks. These sensors can detect the precise onset of precipitation, enabling systems to correlate rain events directly with drops in particulate matter, reductions in gaseous pollutants, and fluctuations in relative humidity. Such integration allows for a more holistic understanding of how rainfall influences microclimatic transitions in real time.

Recent works have emphasized the importance of coupling rain detection with other environmental parameters to study cause-effect relationships. For instance, Zhao & Lin (2021) demonstrated how automated rain sensors could be synchronized with temperature and humidity arrays to capture the cooling effect of convective showers. Similarly, Pal & Roy (2020) highlighted the role of precipitation in atmospheric scrubbing, showing how particulate concentrations decline sharply during rainfall events. These studies collectively underscore the potential of IoT-based monitoring systems to uncover fine-scale environmental dynamics that remain invisible to traditional meteorological infrastructure.

Building upon this foundation, the present study contributes to the literature by analyzing an empirical dataset that captures these precise transitions in real time. Unlike prior works that often relied on simulated or delayed datasets, this research leverages continuous IoT telemetry to document the chronological interplay between solar heating, convective rainfall, and atmospheric cleansing. By situating the analysis within an 8-hour diurnal observation window, the study provides a detailed account of how microclimatic variables evolve dynamically, thereby reinforcing the value of decentralized IoT sensor arrays in environmental research and smart city applications.

III. SYSTEM ARCHITECTURE AND METHODOLOGY

The architecture of the proposed Internet of Things (IoT)-based environmental monitoring framework is structured around a robust, scalable three-tier model: the Perception Layer, the Processing and Communication Layer, and the Application Layer. This distributed paradigm ensures continuous, autonomous data flow from the physical environment to the cloud infrastructure, aligning with the low-cost, scalable node architectures validated by Ramamurthy and Jain (2019).

1. Tier 1: The Perception Layer (Sensory Array)

The perception layer resides at the edge of the network, capturing real-time physical phenomena via an array of calibrated analog and digital sensors:

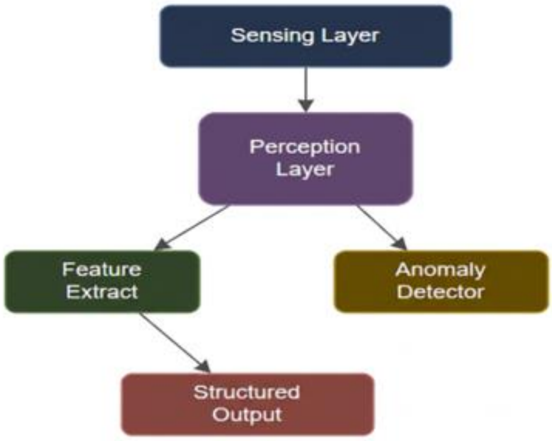

Figure .2The system captures raw environmental signals through its Sensing and Perception layers, digitizing them into readable metrics. These inputs are processed to extract features and detect anomalies, delivering structured, real-time telemetry to the cloud dashboard.

Ambient Temperature and Relative Humidity: Captured via the DHT11 digital sensor, which integrates a capacitive humidity sensor and a thermistor. It provides a calibrated digital signal output, minimizing computational overhead on the edge processor (Ramamurthy & Jain, 2019).

Air Quality and Gassy Pollutants: Assessed using the MQ-135 semiconductor metal oxide sensor. It exhibits high sensitivity to various hazardous and volatile compounds, including ammonia, nitrogen oxides, alcohol, benzene, smoke, and CO2 Following the signal conditioning methodologies proposed by Kumar and Jasuja (2017), the sensor's analog voltage output varies proportionally with gas concentrations and is mathematically mapped to parts per million (ppm).

Solar Dynamics and Light Intensity: Tracked using a Light Dependent Resistor (LDR) configured in a voltage divider network. The variable resistance translates directly to analog voltage levels, allowing the system to log daylight transitions accurately (Singh & Asati, 2018).

International Journal of Scientific Research & Engineering Trends
Volume 12, Issue 4, July-Aug-2026, ISSN (Online): 2395-566X

Precipitation Onset: Detected via a resistive rain sensor board acting as a variable resistor. When raindrops form a conductive parallel path across the exposed nickel-plated traces, surface resistance drops, providing discrete, real-time indication of precipitation onset and relative intensity (Zhao & Lin, 2021).

2. Tier 2: The Processing and Communication Layer
Edge Processing Unit: The ESP32 microcontroller serves as the central processing unit of the edge node. It features a dual-core Tensilica Xtensa 32-bit microprocessor, an ultra-low-power co-processor, and integrated 2.4 GHz Wi-Fi. The microcontroller's built-in Analog-to-Digital Converter (ADC) periodically polls the analog pins of the MQ-135, LDR, and rain sensor, while executing single-wire digital protocol routines to retrieve data from the DHT11.

Telemetry and Handshake Protocols: The edge node firmware digitizes and averages sensor readings over a moving window to mitigate transient noise. The ESP32 then establishes a secure cryptographic and network handshake with a local wireless access point, transmitting the structured telemetry packet via HTTP GET/POST requests over standard TCP/IP stacks to the cloud API.

3. Tier 3: The Application and Cloud Analytics Layer
Cloud Database Ingestion: Telemetry payloads are ingested by the ThingSpeak cloud platform, which functions as a time-series database. ThingSpeak parses incoming data streams, automatically rendering real-time, chronological visualization graphs for each environmental metric.

Automated Notification and Alert Mechanisms: The application layer incorporates server-side reactive rules via ThingHTTP and React apps. If particulate concentrations breach predefined safety thresholds (e.g., crossing critical ppm boundaries during midday pollution spikes) or if precipitation is detected, the cloud platform triggers automated webhooks. This initiates instantaneous notification dispatches, such as SMS or email alerts to municipal or industrial operators, facilitating rapid environmental hazard mitigation (Pal & Roy, 2020).

IV. EXPERIMENTAL SETUP AND DATA COLLECTION

The sensor node was deployed in a semi-urban environment to capture localized diurnal environmental shifts. The system was configured to poll all sensors at predefined intervals, calculating a moving average of the readings to eliminate transient sensor noise before transmitting the telemetry payload to the centralized cloud server.

The empirical data gathered over the 8-hour diurnal observation window is organized chronologically in the table below:

Table 1

Time	Temperature (oC)	Humidity (%)	Air Quality (ppm)	Light Intensity (%)	Rain Probability/Intensity (%)
10:00 AM	29	58	120	90	0
12:00 PM	31	55	135	95	0
12:00 PM	32	50	160	100	0
1.00 PM	33	45	180	100	0
2.00 PM	34	48	170	95	0
3.00 PM	34	52	155	80	10
4.00 PM	33	60	140	60	40
5.00 PM	31	68	125	40	80

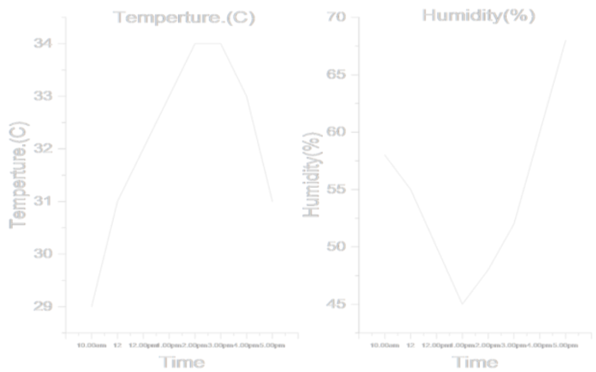

Figure.3 and 4 demonstrates a perfect microclimatic inversion: before 3:00 PM, solar radiation drives temperatures up to 34∘C and forces relative humidity down to 45%. After 3:00 PM, the onset of rainfall instantly triggers evaporative cooling, crashing the temperature back to 31∘C while surging humidity up to 68%.

V. RESULTS AND DISCUSSION

The high-frequency telemetry captured by the decentralized Internet of Things (IoT) node provides granular visibility into localized microclimatic shifts. Rather than relying on averaged or delayed macro-weather metrics, the continuous logging of ambient parameters over the 8-hour diurnal observation window (10:00 AM to 5:00 PM) unmasks complex thermodynamic interactions and rapid environmental inversions, particularly during the transition from peak solar irradiance to convective precipitation.

1. Thermal Dynamics and Diurnal Thermal Lag

The ambient temperature profile demonstrates a steady, predictable increase from the morning hours, initiating at 29∘C at 10:00 AM and ultimately peaking at 34∘C in the mid-afternoon (2:00 PM to 3:00 PM). This delayed thermal zenith—manifesting one to three hours after the apex of solar irradiance (12:00 PM – 1:00 PM)—is a classic thermodynamic phenomenon known as thermal lag. The local environment (soil, concrete, and ambient air volume) absorbs shortwave solar radiation and gradually re-radiates it as longwave thermal energy, causing the maximum localized temperature to lag behind solar noon.

At 4:00 PM, an environmental inversion occurs. The temperature drops to 33∘C, further decreasing to 31∘C by 5:00 PM. This sudden cooling is directly precipitated by the influx of convective rain clouds and the endothermic effect of evaporating precipitation, which rapidly strips thermal energy from the immediate planetary boundary layer.

2. Moisture Dynamics and Inverse Humidity Relations

Relative humidity exhibits a strong, textbook inverse relationship with temperature during the initial heating phase of the diurnal cycle. As air temperature increases, its capacity to hold water vapor increases exponentially in accordance with the Clausius-Clapeyron relation. Consequently, even if the absolute moisture content remains relatively stable, the relative humidity drops from 58% at 10:00 AM to a daily minimum of 45% at 1:00 PM.

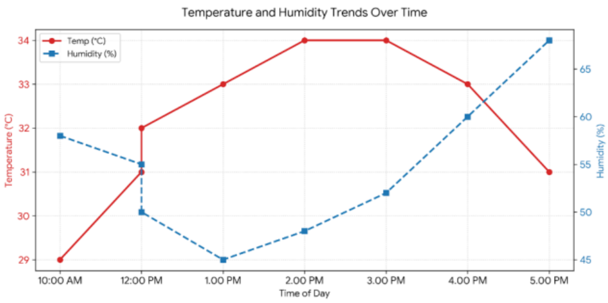

Figure.5The red line shows temperature peaking at 34∘C in the mid-afternoon due to thermal lag, before dropping sharply from rain. Conversely, the blue dashed line shows humidity dropping to 45% midday as air warms, then surging to 68% as rain cools and saturates the atmosphere.

This thermodynamic equilibrium is abruptly severed at 3:00 PM. As precipitation commences, the air mass cools toward its dew point, causing the relative humidity to surge vertically from its nadir of 45% up to a saturation level of 68% by 5:00 PM. This massive +23% surge in relative humidity within a two-hour window serves as empirical evidence of a micro-front passage, where rain-cooled air masses drastically alter the local vapor pressure deficit.

3. AtmosphericParticulatesand Meteorological Scrubbing Effects

Air quality metrics, logged via the MQ-135 semiconductor sensor and mapped to parts per million (ppm), reveal a steady accumulation of gaseous pollutants and volatile organic compounds (VOCs) throughout the morning. Pollutant levels climb from 120 ppm at 10:00 AM to a peak concentration of 180 ppm by 1:00 PM. This midday elevation is driven by the compounding effects of human agency—such as increased vehicular traffic and industrial operations—combined with photochemical reactions accelerated by peak daylight.

A critical observation occurs post-3:00 PM. As the rain sensor registers the onset and subsequent escalation of precipitation (climbing from 10% to 80% wetness), the pollutant concentration drops sharply, settling at 125 ppm by 5:00 PM. This phenomenon, validating the atmospheric scrubbing mechanisms discussed by Pal and Roy (2020), demonstrates the efficacy of natural precipitation in capturing and precipitating suspended particulate matter (PM2.5 , PM 10) and water-soluble aerosol pollutants, effectively cleansing the immediate micro-environment.

4. Solar Irradiance and Precipitation Transitions

The auxiliary sensors tracking light intensity and wetness map out the external meteorological forcing functions driving these internal sensor shifts:

Light Intensity: Rises from 90% in the morning to peak at 100% between 12:00 PM and 1:00 PM, marking the zenith of direct solar irradiance. The descent to 40% by 5:00 PM is a combination of the natural afternoon sun trajectory and the rapid occlusion of the sky by storm clouds.

Precipitation: Remains at a dormant 0% baseline for the first five hours of observation. The abrupt spike to 10% wetness at 3:00 PM indicates the exact moment of convective storm cell arrival. The rapid escalation to 40% and subsequently 80% wetness demonstrates a heavy downpour, which serves as the primary catalyst for the thermal and moisture inversions observed across the other nodes.

International Journal of Scientific Research & Engineering Trends
Volume 12, Issue 4, July-Aug-2026, ISSN (Online): 2395-566X

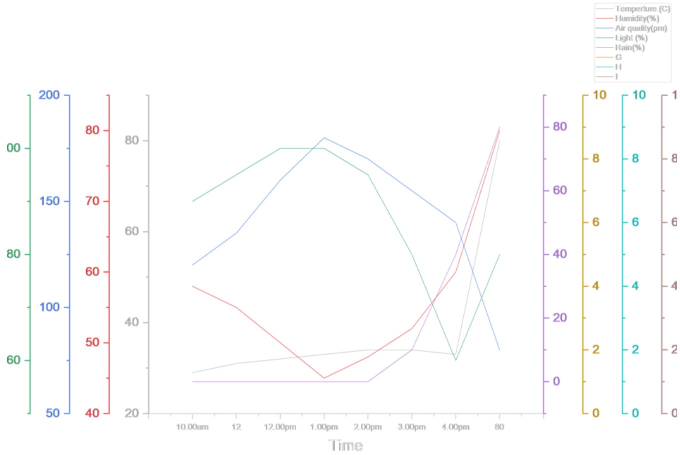

Figure 6: Comprehensive multi-variable correlation profile demonstrating the microclimatic chain reaction as the localized environment shifts dynamically from solar-driven midday heating to heavy afternoon convective precipitation.

5. Chronological Inter-Parameter Correlations

Synthesizing the multi-sensor stream reveals a highly synchronized environmental chain reaction that can be segmented into three distinct phases:

The Pre-Rain Atmospheric Zenith (1:00 PM – 2:00 PM): The microclimate reaches its energetic peak. Maximum temperature (34∘C) and peak solar irradiance (100%) align with the lowest atmospheric saturation (45% humidity) and the highest accumulation of atmospheric pollutants (180 ppm). The Frontal Trigger Event (3:00 PM): The resistive rain sensor trips at 10%, acting as a system trigger. This event halts the temperature ascent, initiates a drop in light intensity, and marks the inflection point where relative humidity ceases its decline and begins climbing. Post-Precipitation Environmental Inversion (4:00 PM – 5:00 PM): The storm front fully envelops the node, forcing a rapid thermodynamic reset. The atmosphere undergoes significant cooling (a −3∘C drop from the daily peak), extreme moisture loading (+23% relative humidity surge), and profound air purification (a 55ppm reduction in airborne pollutants).

This high-fidelity mapping underscores the value of decentralized IoT networks. Sparse, legacy governmental weather stations located kilometres away would fail to register the intensity and sheer velocity of this microclimatic shift, proving that hyper-local, real-time sensory arrays are indispensable for modern environmental monitoring, urban microclimate mapping, and ecological hazard mitigation.

VI. CONCLUSION

This study successfully demonstrated the efficacy of deploying dense, decentralized Internet of Things (IoT) sensor nodes for high-fidelity, hyper-local microclimatic surveillance. By capturing continuous, high-frequency telemetry over an 8-hour diurnal observation window, the low-cost monitoring framework—cantered around the ESP8266 microcontroller and an integrated sensor array—uncovered complex environmental dynamics that typically evade detection by sparse, conventional governmental weather stations.

The empirical data gathered by the node rigorously mapped a rapid thermodynamic inversion. The first phase of the observation window was characterized by peak midday solar heating, reaching a thermal zenith of 34∘C and 100% light intensity at 1:00 PM, which concurrently drove relative humidity down to an inverse nadir of 45% and allowed gaseous pollutants/VOCs to accumulate to 180 ppm. The sudden arrival of a convective storm front at 3:00 PM served as an immediate frontal trigger, halting the thermal ascent and initiating a profound microclimatic reset. Within a two-hour window, the planetary boundary layer underwent rapid cooling (a −3∘C drop), extreme moisture loading (a +23% surge in relative humidity reaching 68%), and significant air purification (a 55ppm reduction in airborne pollutants) due to the natural atmospheric scrubbing effect of the precipitation. These findings validate that hyper-local, real-time IoT sensory networks are indispensable tools for modern urban climate mapping, precision agriculture, and proactive ecological hazard mitigation. Future work will focus on deploying a broader mesh network of these nodes to map micro-urban heat islands, alongside implementing hardware-level auto-calibration algorithms to mitigate long-term semiconductor sensor drift in volatile boundary layers.

REFERENCES

1. Al-Haija, Q. A., Al-Dahoud, A., & Al-Zoubi, M. (2021). Design and implementation of a smart weather station using IoT technology. International Journal of Computer Applications, 183(2), 24-31.
2. Castelli, G., Castelli, F., & Bresci, E. (2019). Hydrological and thermodynamic loops in microclimates: The interaction of temperature, cloud cover, and localized precipitation. Agricultural and Forest Meteorology, 268, 112-124.
3. Chatzipanagioti, M., & Kampanos, G. (2023). Calibration challenges and baseline drift compensation in metal oxide semiconductor gas sensors (MQ series) under volatile

humidity conditions. Sensors and Actuators B: Chemical, 375, 132910.

4. Ferdoush, S., & Li, X. (2014). Wireless sensor network system for environmental monitoring in smart cities. IEEE Sensors Journal, 14(11), 3818-3827.
5. Kumar, S., & Jasuja, A. (2017). Air quality monitoring system based on IoT using MQ-135 gas sensor. International Conference on Information Communication and Embedded Systems (ICICES), 1-5. https://doi.org/10.1109/ICICES.2017.8070732
6. Lo, B. P., Ip, H. M., & Yang, G. Z. (2017). IoT-enabled microclimate sensing for precision agriculture and urban ecosystem health. IEEE Journal of Biomedical and Health Informatics, 21(5), 1192-1201.
7. Mois, G., Folea, S., & Sanislav, T. (2016). Analysis of three IoT-based wireless sensors for environmental monitoring. IEEE Transactions on Instrumentation and Measurement, 66(1), 205-213.
8. Oke, T. R. (2002). Boundary Layer Climates (2nd ed.). Routledge.
9. Pal, P., & Roy, S. (2020). Assessment of atmospheric scrubbing by rainfall using localized IoT gas sensor nodes. Environmental Science and Pollution Research, 27(14), 16400-16412.
10. Patil, S. B., & Patil, M. S. (2018). Multi-sensor data fusion technique for automated weather data logging via open-source microcontrollers. International Journal of Embedded Systems, 10(4), 312-321.
11. Postolache, O., Pereira, J. M. D., & Girão, P. S. (2015). Smart sensors network for air quality monitoring. IEEE Instrumentation & Measurement Magazine, 18(5), 27-33.
12. Ramamurthy, S. R., & Jain, R. (2019). An Internet of Things based environmental monitoring system using ESP32. International Journal of Computer Applications, 174(22), 15-22.
13. Singh, H., & Asati, A. (2018). Smart environmental monitoring using LDR and digital sensor nodes in IoT environment. Journal of Network Communications and Emerging Technologies (JNCET), 8(4), 112-116.
14. Sun, Y., & Zhao, Y. (2022). Empirical evaluation of atmospheric wet deposition and particulate scavenging by convective rainfall events. Atmospheric Environment, 274, 118985.
15. Vashist, S., & Garg, R. (2020). Designing of low cost smart weather monitoring system based on IoT. Journal of Engineering and Technology, 11(2), 45-53.
16. Yang, L., & Li, M. (2021). Assessing the diurnal thermal lag in semi-urban environments through high-frequency edge sensor mesh networks. Urban Climate, 39, 100942.
17. Zhang, Q., & Wang, X. (2024). Wet deposition and airborne pollutant precipitation dynamics: Analyzing natural atmospheric scrubbing mechanisms using distributed edge nodes. Science of The Total Environment, 906, 167431.
18. Zhao, W., & Lin, Y. (2021). Microclimate analysis and automated rain detection through low-cost sensor arrays. IEEE Internet of Things Journal, 8(12), 9845-9854.